Realistic modeling of surface seismic and VSP using DAS with straight and shaped fibers of variable gauge length

Anton Egorov and Marwan Charara, Aramco Research Center - Moscow, Aramco Innovations LLC;
Ezzedeen Alfataierge and Andrey Bakulin, EXPEC Advanced Research Center, Saudi Aramco

Summary

There is a rising demand for distributed acoustic sensing (DAS) in exploration and developmental geophysics. DAS has several advantages over conventional sensors, for example, fine spatial sampling, wide frequency range, relative ease of permanent downhole deployment. A few examples of using shaped cables were recently presented, which improve the broadside sensitivity of DAS systems. We present a pseudospectral algorithm that can model the seismic gathers acquired with straight and helical cables with DAS systems. The use of an accurate wavefield interpolation technique allows us to obtain synthetic wavefields with fine spatial sampling. The fit-for-purpose strain averaging methodology models the response of shaped fibers and the gauge length's smoothing effect in a consistent manner. We model DAS seismic gathers for surface and borehole seismic acquisitions, examine their properties, and compare them to the more conventional particle velocity recordings.

Introduction

An accurate seismic data modeling engine is a must for survey design and seismic processing with geophones. Likewise, the algorithms for modeling seismic data acquired by distributed acoustic sensors (DAS) need to be developed before the DAS acquisition becomes a routine. We present our method for such modeling. We compute and analyze the seismic gathers for different acquisition types: surface seismic with buried cables and borehole VSP surveys.

DAS systems employ a device called an interrogator, which transmits a light pulse through a fiber segment and analyses the backscattered light, reconstructing the strain along the fiber averaged over a specific interval called the gauge length (Parker et al., 2014). The use of finite gauge length implies that the DAS sensor always acts as a seismic array. DAS systems with straight fibers have poor broadside sensitivity, i.e., they are insensitive to the *P*-waves that travel perpendicular to the direction of the fiber. Thus, such systems are mainly used for VSP (e.g., Mateeva et al., 2014), although the concept of distributed sensing has much potential for surface seismic (Bakulin et al., 2020). Kuvshinov (2016) suggests using helically wound cables to gain broadside sensitivity, which could potentially be employed for surface seismic. Such cables have been successfully tested in the field. However, it turns out that, at least in some cases, their response for onshore deployments may strongly change with the season (Tertyshnikov et al., 2020). Innanen (2017a) suggests a more complex nested helix geometry for even better recording of broadside wavefields.

The response of a DAS system with a straight fiber is, in most cases, modeled as a component of the strain tensor along the cable smoothed by a filter of choice to simulate the effects of gauge length (and pulse width) (Dean et al., 2017; Podgornova et al., 2017). For most finite-difference codes (Cartesian or cylindrical), the vertical component of the strain tensor ε_{zz} is easy to compute. For a non-vertical well, the strain tensor needs to be rotated in order to compute the tangential strain component along the wellbore. For shaped fibers, Innanen (2017b) provides a parameterization, which can be used for the computation of tangential strains. Using this parameterization, Eaid et al. (2020) develop a forward engine for modeling of seismic data acquired with shaped DAS sensors and conduct an elastic full-waveform inversion of the generated data. We use the same parameterization and develop a 2D modeling engine that considers the gauge length effects. We demonstrate DAS modeling for surface seismic and VSP acquisition.

Method

We use the 2D pseudospectral seismic modeling method for elastic wave equation (Fornberg, 1987). The pseudospectral method allows using large grid cells, which may significantly speed up the computation of wavefields at the cost of an accuracy loss for models with strong contrasts. Wavefield interpolation is required to enable the modeling of gathers with realistic receiver sampling for DAS systems. To enable the recording of wavefields at any spatial location, we apply Kaiser windowed sinc functions (Hicks, 2002). This allows us to obtain fine receiver sampling and model seismic gathers acquired with curved cables, computing wavefields between the grid points with minimal cost.

For the computation of DAS system response, we follow the algorithm by Eaid et al. (2020) with slight modifications in gauge length effect modeling. We first compute the strain tensor ε_{ij} at the selected receiver locations. Next, this tensor needs to be rotated to a coordinate system connected to the fiber, and the tangential component of the rotated tensor along the fiber, ε_{tt}, needs to be extracted. For any point s on the fiber this can be computed as follows:

$$\varepsilon_{tt}(s) = (\hat{\mathbf{t}}\cdot\hat{\mathbf{x}})^2\varepsilon_{xx} + (\hat{\mathbf{t}}\cdot\hat{\mathbf{y}})^2\varepsilon_{yy} + (\hat{\mathbf{t}}\cdot\hat{\mathbf{z}})^2\varepsilon_{zz} + 2(\hat{\mathbf{t}}\cdot\mathbf{x})(\hat{\mathbf{t}}\cdot\hat{\mathbf{y}})\varepsilon_{xy} + 2(\hat{\mathbf{t}}\cdot\mathbf{y})(\hat{\mathbf{t}}\cdot\mathbf{z})\varepsilon_{yz} + 2(\hat{\mathbf{t}}\cdot\mathbf{x})(\hat{\mathbf{t}}\cdot\hat{\mathbf{z}})\varepsilon_{xz}. \quad (1)$$

Here $(\hat{\mathbf{x}}, \hat{\mathbf{y}}, \hat{\mathbf{z}})$ is the Cartesian coordinate system used in the code, and $\hat{\mathbf{t}}$ is the tangent vector to the fiber at the point s (Figure 1). It is important to note that even in our 2D code, the helical fiber geometries are considered in 3D, but some terms in equation (1) become zeroes due to the strain components ε_{xy}, ε_{yy} and ε_{yz} being equal to zero.

The DAS response $d(s)$ can be modeled by averaging the computed ε_{tt} in a symmetric window:

$$d(s) = \int_{-\infty}^{\infty} W(s - s', L)\varepsilon_{tt}(s')ds', \quad (2)$$

where $W(s, L)$ is a rectangular window around s with half-width $L/2$, L is the gauge length. This effectively means that each of the terms in (1) needs to be averaged before summation.

It is not feasible to compute (2) directly – fiber loops for a helical fiber are a few centimeters long, which would require fine spatial sampling of strains. Eaid et al. (2020) assume strains being constant within the gauge length, which leads to equation (1) being transformed into (we keep only the 2D terms):

$$d(s) = \varepsilon_{xx}A_{xx} + \varepsilon_{zz}A_{zz} + \varepsilon_{xz}A_{xz}, \quad (3)$$
$$A_{ii} = \frac{1}{L}\int_{s-L/2}^{s+L/2} \hat{t}_i(s')^2 ds'; A_{xz} = \frac{2}{L}\int_{s-L/2}^{s+L/2} \hat{t}_x(s')\hat{t}_z(s')ds'.$$

A_{ii} are the summation coefficients for corresponding strain components. This representation allows for capturing directivity differences of straight and helical cables. However, it disregards the strain-smoothing effect of the gauge length due to constant-strain approximation. For example, for a straight vertical cable $d(s) == \varepsilon_{zz}(s)$ in this approximation.

Instead, we assume that the strain changes slowly within the gauge length. We pick a receiver sampling interval R that is small relative to gauge length (thinking about field seismic acquisition with 5-20 m gauge lengths, this interval is 1 or 0.5 m). The characteristic size of a shaped fiber, e.g., fiber loop, needs to be much smaller than R. We then conduct the averaging in two stages. First, we do the same averaging as in equation (3), but only within $\pm R/2$ and only for the selected receiver locations. For a helical cable, these locations are equally spaced points on the cable core c. For every picked location c, we choose the closest point on the fiber s for the following averaging:

$$\overline{\varepsilon_{tt}}(c) = \varepsilon_{xx}A^R_{xx} + \varepsilon_{zz}A^R_{zz} + \varepsilon_{xz}A^R_{xz}, \quad (4)$$
$$A^R_{ii} = \frac{1}{R}\int_{s-R/2}^{s+R/2} \hat{t}_i(s')^2 ds'; A^R_{xz} = \frac{2}{R}\int_{s-R/2}^{s+R/2} \hat{t}_x(s')\hat{t}_z(s')ds'.$$

The averaged $\overline{\varepsilon_{tt}}$ already has the inherent directivity characteristics of a shaped fiber (e.g., it will have broadside sensitivity for a helical fiber). Next, $\overline{\varepsilon_{tt}}$ is averaged within the desired gauge length to obtain the modified DAS response:

$$\bar{d}(c) = \int_{-\infty}^{\infty} W(c - c', \dot{L})\overline{\varepsilon_{tt}}(c')dc'; \dot{L} = L/\alpha. \quad (5)$$

Here, α is fiber-to-cable length ratio, which is needed because we move from averaging over the cable s to averaging over the cable core c – this accounts for the fact that, for the shaped fibers, the gauge length of L m will cover L/α m of cable. $\bar{d}(c)$ provided by the equation (5) will take into account both the directivity characteristics set by the fiber shape and the inherent gauge length smoothing effect – for the same vertical fiber case, $\bar{d}(c)$ will be equal to ε_{zz} averaged in a symmetric window of size L.

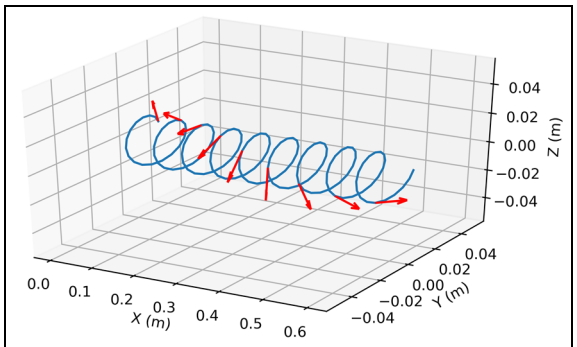

Figure 1: An example of helical DAS geometry with tangent vectors displayed.

Results – surface geometry

First, we test the algorithm on the elastic Marmousi model with surface receivers (note that water was replaced by a solid, i.e., the model has nonzero shear wave velocity everywhere). Figure 2a shows the *P*-wave velocity for the model with locations of the source and the receivers displayed (the receiver locations for the following VSP example are also shown). The free surface is active, the source and receivers are 25 m below the surface, Ricker wavelet with 25 Hz dominant frequency is used. Figures 2b-d contain straight DAS, helical DAS with 35.3° lead angle, and vertical particle velocity gathers respectively. As expected, the straight DAS is not sensitive to broadside *P*-waves and does not record reflections at small offsets. The helical cable provides the broadside sensitivity and records the reflections similar to those recorded by vertical particle velocity sensors. Note that the lead angle of the helical cable was chosen on purpose such that the cable is insensitive to the shear waves (Baird, 2020). Still, some slow events can be observed in Figure 2c, which we believe are caused by the interaction of the wavefield with the free surface.

DOI:10.1190/segam2021-3576626.1

Results – vertical seismic profile

Figure 3 displays the seismic gathers computed for the VSP acquisition in the same model (well location is displayed in Figure 2a, source offset from the well is 2 km, 40 Hz Ricker wavelet was used). First, we compare the vertical particle velocity gather (Figure 3a) with the strain component ε_{zz} (Figure 3b). We can observe that these gathers are similar. Indeed, their difference manifests itself in the opposite signs of the downgoing wavefields and slightly different broadside sensitivity, $cos(\Theta)$ for particle velocity versus $cos^2(\Theta)$ for ε_{zz}, where Θ is the angle of incidence. The DAS gathers in Figures 3c and 3d are essentially the ε_{zz} smoothed by two different gauge lengths. Though the gathers for ε_{zz} and straight DAS with 10 m gauge length look similar, the analysis of their amplitude spectra (Figure 4) shows the lower level of high frequencies for DAS gather, which is caused by the DAS array-driven averaging along the cable. For the 30 m gauge length, the averaging is even stronger and can be observed on the gather itself.

When analyzing the helical cable data in Figure 3e, we can observe the absence of *S*-waves, both source-generated and converted (examples of *P*- and *S*-wave reflections are highlighted on the gathers). This suggests a few potential applications. First, a purely acoustic FWI in conjunction with land data may be possible for such a cable resembling a land hydrophone (Burnstad et al., 2013). Second, cables of different shapes (e.g., straight and helical) can be jointly used in various processing and inversion algorithms. Ning and Sava (2018) demonstrated the possibility of estimating the strain tensor using several helical fibers and a straight fiber when the gauge length is small enough. Using a few different cables may help separate reflections and ground roll, assist converted/S-wave imaging, or tackle parameter crosstalk in elastic FWI.

Discussion

The presented methodology allows for the modeling of DAS seismic data with cables of different shapes. The receiver interpolation in the algorithm makes it possible to compute straight and helical DAS data with a small receiver spacing as used in field DAS data acquisition for any shape of the well, which allows for the exact simulation of a planned DAS acquisition geometry. If used for the full-waveform inversion, this type of modeling engine would allow for minimal data preprocessing. For example, Egorov et al. (2018) decimate DAS data to the finite-difference cell size and convert it to particle velocity for full-waveform inversion, removing the gauge length effect. The methodology presented here allows for removing these extra preconditioning steps, thus minimizing the potential errors. While we demonstrated a numerical approach for the computation of DAS gathers using the pseudospectral

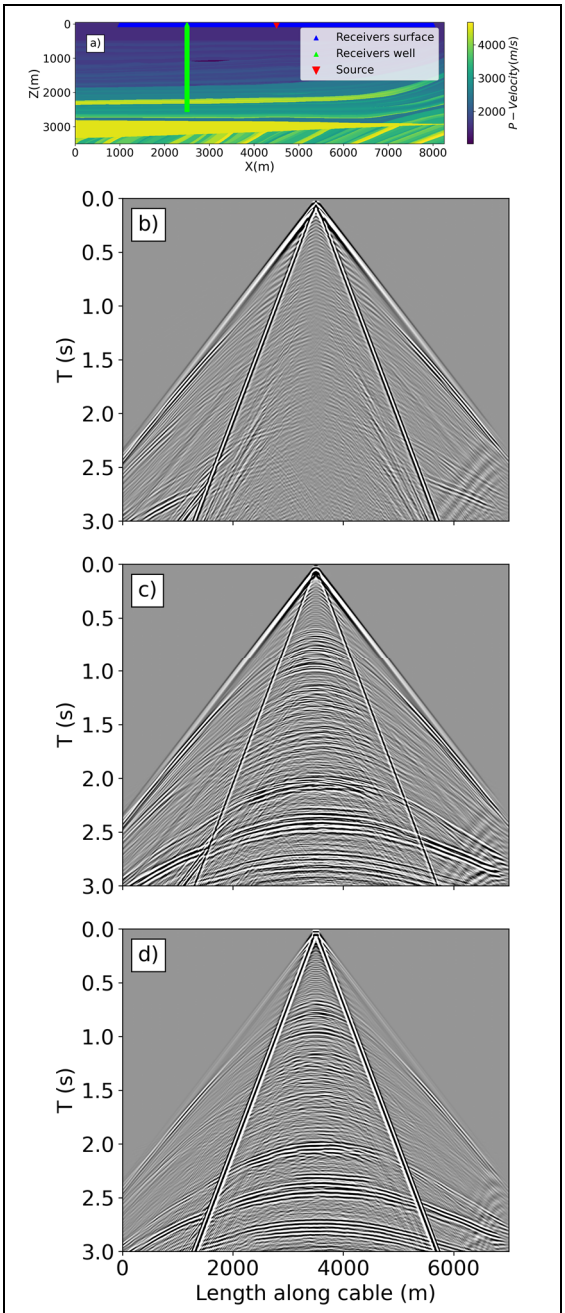

Figure 2: A fragment of the Marmousi model used for the computations (sources and receivers are displayed for surface and the following VSP geometry) (a); seismic gathers recorded with surface receivers: straight DAS (b), helical DAS with 35.3° lead angle (c), geophones (vertical particle velocity) (d). The gauge length for all DAS gathers is equal to 10 m. Reflections visible on geophones (d) and helical DAS (c) are not appearing on straight DAS (b).

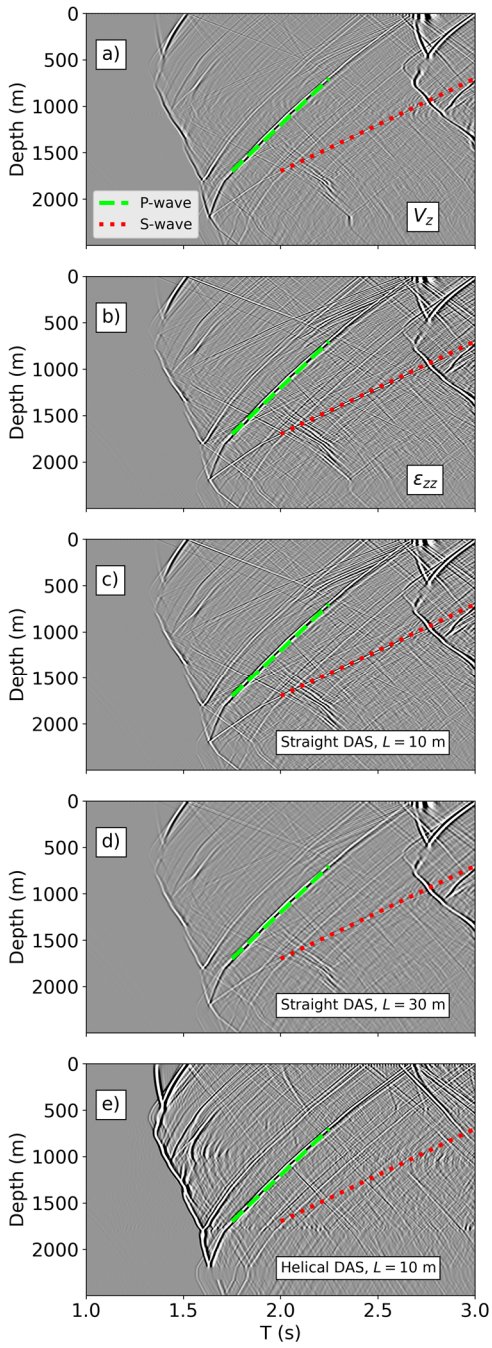

Figure 3: Seismic gathers recorded with VSP receivers: geophones (vertical component of particle velocity) (a), ε_{zz} (b), straight vertical DAS (L=10 m) (c) , straight vertical DAS (L=30 m) (d), helical DAS with 35.3° lead angle (L=10 m) (e).

algorithm, a similar strain averaging method can be implemented as a module inside any finite-difference code.

Conclusions

We present a method for modeling seismic data acquired with distributed acoustic sensors. The critical element of the algorithm is the strain averaging strategy, which allows us to obtain accurate modeling results for variable gauge lengths and fiber shapes. The averaging takes into account the variability of strain field within the gauge length and hence correctly models the smoothing effect induced by the finite gauge lengths. The resulting algorithm can obtain synthetic DAS gathers with gauge length effect taken into account. An accurate wavefield interpolation method provides fine receiver sampling, characteristic of DAS systems, at a relatively low computational cost.

Acknowledgments

The authors would like to thank Pavel Golikov and Mustafa Al Ali (Aramco Research Center - Moscow and Aramco Innovations LLC) for productive discussions on this research topic.

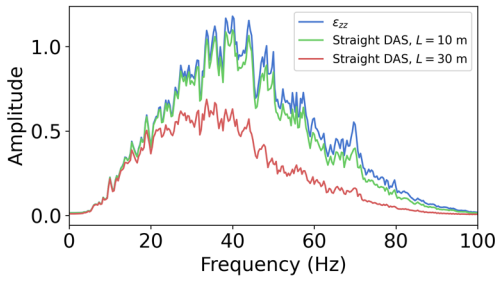

Figure 4: Amplitude spectra of ε_{zz} and straight DAS gathers from Figure 3.

REFERENCES

Baird, A., 2020, Modelling the response of helically wound DAS cables to microseismic arrivals: First EAGE Workshop on Fibre Optic Sensing, Extended Abstracts, WeFOS04, doi: https://doi.org/10.3997/2214-4609.202030019.

Bakulin, A., I. Silvestrov, and R. Pevzner, 2020, Surface seismics with DAS: An emerging alternative to modern point- sensor acquisition: The Leading Edge, **39**, 808–818, doi: https://doi.org/10.1190/tle39110808.1.

Burnstad, R., A. Bakulin, R. Smith, and M. Jervis, 2013, Evaluating new designs of land hydrophones and geophones for permanent monitoring: 83rd Annual International Meeting, SEG, Expanded Abstracts, 4905–4909, doi: https://doi.org/10.1190/segam2013-1020.1.

Dean, T., T. Cuny, and A. H. Hartog, 2017, The effect of gauge length on axially incident P-waves measured using fibre optic distributed vibration sensing: Geophysical Prospecting, **65**, 184–193, doi: https://doi.org/10.1111/1365-2478.12419.

Eaid, M. V., S. D. Keating, and K. A. Innanen, 2020, Multiparameter seismic elastic full-waveform inversion with combined geophone and shaped fiber-optic cable data: Geophysics, **85**, no. 6, R537–R552, doi: https://doi.org/10.1190/geo2020-0170.1.

Egorov, A., J. Correa, A. Bóna, R. Pevzner, K. Tertyshnikov, S. Glubokovskikh, V. Puzyrev, and B. Gurevich, 2018, Elastic full-waveform inversion of vertical seismic profile data acquired with distributed acoustic sensors: Geophysics, **83**, no. 3, R273–R281, doi: https://doi.org/10.1190/geo2017-0718.1.

Fornberg, B., 1987, The pseudospectral method: Comparisons with finite differences for the elastic wave equation: Geophysics, **52**, 483–501, doi: https://doi.org/10.1190/1.1442319.

Hicks, G. J., 2002, Arbitrary source and receiver positioning in finite-difference schemes using Kaiser windowed sinc functions: Geophysics, **67**, 156–165, doi: https://doi.org/10.1190/1.1451454.

Innanen, K., 2017a, Determination of seismic-tensor strain from Helical Wound Cable-Distributed Acoustic Sensing cable with arbitrary and nested-helix winds: 87th Annual International Meeting, SEG, Expanded Abstracts, 926–930, doi: https://doi.org/10.1190/segam2017-17664060.1.

Innanen, K., 2017b, Parameterization of a helical DAS fibre wound about an arbitrarily curved cable axis: 79th Conference and Exhibition, EAGE, Extended Abstracts, We A5 15, doi: https://doi.org/10.3997/2214-4609.201701202.

Kuvshinov, B. N., 2016, Interaction of helically wound fibre-optic cables with plane seismic waves: Geophysical Prospecting, **64**, 671–688, doi: https://doi.org/10.1111/1365-2478.12303.

Mateeva, A., J. Lopez, H. Potters, J. Mestayer, B. Cox, D. Kiyashchenko, P. Wills, S. Grandi, K. Hornman, B. Kuvshinov, W. Berlang, Z. Yang, and R. Detomo, 2014, Distributed acoustic sensing for reservoir monitoring with vertical seismic profiling: Geophysical Prospecting, **62**, 679–692, doi: https://doi.org/10.1111/1365-2478.12116.

Ning, I. L. C., and P. Sava, 2018, High-resolution multi-component distributed acoustic sensing: Geophysical Prospecting, **66**, 1111–1122, doi: https://doi.org/10.1111/1365-2478.12634.

Parker, T., S. Shatalin, and M. Farhadiroushan, 2014, Distributed Acoustic Sensing – a new tool for seismic applications: First Break, **32**, 61–69, doi: https://doi.org/10.3997/1365-2397.2013034.

Podgornova, O., S. Leaney, S. Zeroug, and L. Liang, 2017, On full-waveform modeling and inversion of fiber-optic VSP data: 87th Annual International Meeting, SEG, Expanded Abstracts, 6039–6043, doi: https://doi.org/10.1190/segam2017-17652912.1.

Tertyshnikov, K., G. Bergery, B. Freifeld, and R. Pevzner, 2020, Seasonal effects on DAS using buried helically wound cables: EAGE Workshop on Fiber Optic Sensing for Energy Applications in Asia Pacific, doi: https://doi.org/10.3997/2214-4609.202070007.